FILE

INTERNAL DOCUMENT 181

I.O.S.

THE IMAGING OF WAVES BY SATELLITE-BORNE SYNTHETIC APERTURE RADAR: THE EFFECTS OF SEA SURFACE MOTION

by

M J TUCKER

NATURAL ENVIRONMENT RESEARCH COUNCIL

INSTITUTE OF OCEANOGRAPHIC SCIENCES

INSTITUTE OF OCEANOGRAPHIC SCIENCES

Wormley, Godalming,
Surrey GU8 5UB
(042-879-4141)

(Director: Dr. A. S. Laughton)

Bidston Observatory,
Birkenhead,
Merseyside L43 7RA
(051-653-8633)
(Assistant Director: Dr. D. E. Cartwright)

Crossway,
Taunton,
Somerset TA1 2DW
(0823-86211)
(Assistant Director: M. J. Tucker)

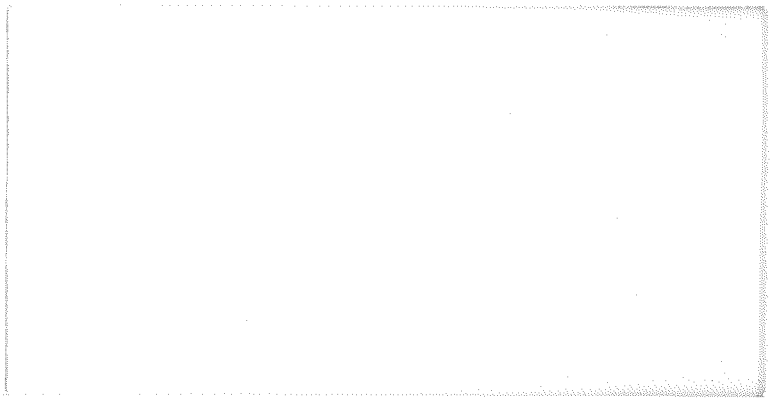

THE IMAGING OF WAVES BY SATELLITE-BORNE SYNTHETIC APERTURE RADAR: THE EFFECTS OF SEA SURFACE MOTION

by

M J TUCKER

Internal Document No 181

Institute of Oceanographic Sciences
Crossway,
Taunton, Somerset

1983

ABSTRACT

The effects of sea-surface velocities in the imaging of waves by synthetic aperture radar are considered. One essential initial concept is that of a primary scene element, which is a small patch of seas surface which can be considered to have a constant target strength during the SAR integration. It is then shown that if the sea wave spectrum is divided at the nominal limit of resolution of the SAR the effect of the long and short wavelength parts can be considered separately, the former being treated by numerical simulation, the latter by statistical methods. It is found that the short wavelengths produce an azimuthal smearing which can be represented by a Gaussian low-pass filter acting on the azimuthal component of wavenumber in the image. The cut-off wavelength is typically some hundreds of metres in moderate winds. Images obtained with the Seasat-SAR frequently show such an effect.

NOTATION

σ	the backscattering cross-section per unit area of sea surface
σp	the actual value including the random variation
σ_e	the expected value of σp (the mean of the probability distribution)
σ_o	the average value of σ_e over an area containing many sea wavelengths
$s(x,y) = \{\sigma(x,y)-\sigma_o\}/\sigma_o$	the image intensity of a SAR scene
$s'(x,y)$	as $s(x,y)$ but after processing
$R(k_x)$	the response factor due to SAR processing
v_r	the range component of the velocity of a target
$p(v_r)$	the probability density of v_r
μ	the rms value of v_r
χ	the azimuthal offset
ν	the rms value of χ
R_s	the range of the target from the radar
V_s	the radar platform velocity
ρ	the resolution of the SAR (assumed to be the same in range and azimuth)
θ_i	the angle of incidence of the radar on the sea surface
λ_R	the wavelength of the radar carrier
λ_B	the corresponding Bragg resonant wavelength
λ_1	the upper limit of integration (sea wavelength)
k_x, k_y	the components of the sea wave number $k = 2\pi/\lambda$
ζ	the elevation of the sea surface above the mean level
$S(\omega)$	the spectral density of the sea wave system at ω
ω	2π x the frequency
Ω_1 Ω_2	limits of integration
g	the acceleration due to gravity
α	a non-dimensional constant in the Phillips and Pierson-Moskowitz spectral formulations
β	a non-dimensional constant in the Pierson-Moskowitz spectral formulation
U	the wind speed at a height of 19.5 m above the sea surface in m/s
$v(t)$	a signal voltage
$r(\tau)$	the auto-correlation of $v(t)$ with a time delay of τ
$< >$	an ensemble average

1. INTRODUCTION

The US satellite Seasat, which operated for a few months in 1978, carried an L-band synthetic aperture radar (SAR) designed for imaging the ocean surface, and in particular for imaging surface waves. The IEEE Journal of Oceanic Engineering had a special issue devoted to the Seasat sensors, and this contains a paper by Jordan (1980) giving details of the SAR. The main parameters relevant to the present discussion were: altitude 800 km; radar wavelength 23.5 cm; angle of incidence (nominal) 20.5°; resolution on the sea surface 25 x 25 m; platform velocity in orbit 7.44 km/s; 4-look integration time 0.62 s.

Seasat imaged waves on many occasions, and when surface measurements were available for comparison, generally gave reasonable agreement for predominant wavelength and direction (at the present time, our knowledge of the imaging mechanism is insufficient to allow derivation of waveheight). However on occasions no wave pattern was visible even though waves were known to be present, and now that digitally-processed images, and digitally processed spectra of these images are becoming available, it is apparent that on many occasions some mechanism is operating which acts as a low-pass filter on the azimuthal component of wavenumber.

Alpers et al (1981) list 53 papers relating to the imaging of sea waves by SAR's, and by now there are many more. It is a difficult problem and in spite of all this effort we can still not relate the wave spectrum to the image spectrum in analytic terms: indeed, there is still considerable discussion as to the nature of some of the physical processes involved.

The concept of aperture synthesis requires the scene to be stationary during the aperture synthesis process, which took 0.62 s in the case of the Seasat SAR, for example. During such a period the sea surface can move several wavelengths, and in general this results in a degradation of the along-track (or "azimuthal") resolution. This problem can be approached from several different points of view, the relationships between them being discussed briefly in section 4.2.

Because the critical process obeys linear equations, the motions of the sea-surface can be divided into three scales: ripples responsible for the primary backscatter, long waves which can in principle be resolved by the SAR, and intermediate wavelengths. Consideration of the latter enables some very significant statements to be made about the effects of sea-surface motion, and this is the principle contribution of the present paper.

For those not familiar with this subject, a good review of the principles of SAR is given by Tomiyasu (1978), and the theory of the imaging of waves by microwave radars is reviewed by Alpers et al (1981). Unless otherwise stated, justification for statements made below about existing knowledge will be found in these papers.

2. THE STEPS IN THE IMAGING PROCESS: GENERAL DISCUSSION

2.1 The production of the primary scattered field

A crucial step in the present paper is to deduce that by choosing a patch of the sea surface whose width is a small number of Bragg resonant wavelengths, its backscattering cross-section can be regarded as constant

during the SAR integration time. This will be justified in section 3. For Seasat-SAR the patch would be perhaps 2 m square, but its precise size and shape are not critical.

If σ_p is the actual backscattering cross-section of such a "primary scene element", the field of σ_p represents the primary scattering field: that is, the real backscattering field before the interactions of surface motions with the aperture synthethis process have taken place. For similar conditions of water surface slope etc, σ_p varies in a random way (the speckle phenomenon) as will be discussed in section 5. The "expected value" σ_e of σ_p is the mean of its probability distribution, and this depends on the values of quantities such as water surface slope governed by the longer waves present. The precise physical processes producing this modulation are not yet fully understood: there is serious discrepancy between theoretical predictions and field measurements using static radars. However, the present paper is not concerned with this aspect of the imaging process. We shall assume that our objective is to produce as accurate an image as possible of the field of σ_e at an instant of time.

2.2 From the primary scattering field to the output of the aperture synthesis

The aperture synthesis process is linear in the sense that the law of superposition applies: if another target is added to the scene, it passes through the aperture synthesis process without affecting the imaging of the other targets present. If there is already another target in the same resolution cell, the complex amplitudes will add (that is, the phases and amplitudes will add vectorially).

Thus, the primary scene elements defined in 2.1 will all pass through the aperture synthesis process independently and can be added in its output

before the detector stage. The implications of this will be examined more thoroughly in section 5.

Each primary scene element is being transported by the particle velocity due to the longer waves present. If v_r is the range component of velocity, then it results in an apparent along track ("azimuthal") offset χ given by

$$\chi = (R_s/V_s)\, v_r \qquad (1)$$

where R_s is the range and V_s is the platform velocity. (The explanation for this can be found in Tomiyasu 1978)

This again is a linear equation, so that if

$$v_r = v_1 + v_2$$

where v_1 and v_2 are due to different components of the wave spectrum, we can write

$$\chi = \chi_1 + \chi_2$$

where

$$\chi_1 = (R_s/V_s)\, v_1$$

$$\chi_2 = (R_s/V_s)\, v_2$$

Thus, in so far as velocity effects are concerned, the various components of the sea wave spectrum can be carried through this stage independently. One of the most useful conclusions of the present paper results from examining the statistics of χ (section 5).

2.3 Stage 3: detection

In the final detection stage, the amplitudes of the various primary scene elements which have finished up in a given resolution cell are added vectorially. The resultant $|\text{amplitude}|^2$ is taken as being proportional to the scattering cross-section of that resolution cell, though the vector resultant can be presented in other ways.

3. THE PRIMARY SCATTERING ELEMENT

3.1 General

The present paper uses the basic two-scale model introduced by Wright (1968) and widely used since (see also Bass et al (1968)). This regards the sea-surface as composed of small effectively planar patches to which the theory of Bragg scattering can be applied, riding over the longer and higher waves present. For the present purpose we need to consider the time-coherence of these patches rather carefully, to see whether they can be regarded as having a constant target strength during the aperture synthesis process. It is also important to get an approximate measure of their size, since we shall be considering the effect on them of much shorter wavelength sea waves than is usual. In effect, we shall be considering a three-scale model: Bragg scatterers, long waves which can in principle be imaged, and the components of the wave spectrum between.

The small patches of Bragg scattering waves will be termed 'Primary scattering elements'. What we are actually talking about, of

course, is the backscattered field due to these elements, which is the primary scene element.

3.2 Bragg scattering theory

When radio waves illuminate a surface whose roughness is small compared to a wavelength, the departures from specular reflection can be calculated by adding a small electromagnetic field which allows the correct conditions to be satisfied at the actual boundary. The theory is given by Wright (1966) (see also Barrick 1972). Since the equations are linear, the response to each component of the wave spectrum can be treated separately and superposed. When the response to the general sinusoidal long-crested wave is calculated, a sharp resonance is found when the wavecrests are parallel to the radar wave front, and when the sea wavelength has a value λ_B given by

$$\lambda_B = \lambda_R/(2 \sin \theta_i) \tag{2}$$

where λ_R is the radar wavelength

θ_i is the angle of incidence of the radar beam

This is the well-known "Bragg resonance"phenomenon.

However, when the roughness of the sea surface becomes comparable with or greater than a radar wavelength, the equations become non-linear and the responses to individual components of the wave spectrum interact in an increasingly complicated way, so that the backscatter is no longer due to an individual Bragg resonant component of the sea wave spectrum.

The validity of the Bragg resonance principle for wave displacements which are small compared to a wavelength is demonstrated when HF radar (radar wavelengths of 10 to 100 m) is backscattered from moderate seas. Using coherent HF radars the Doppler shift due to the velocity of

propagation of the Bragg resonant sea waves can be resolved and gives a very narrow frequency band (typical width <0.01 Hz) at the expected frequency (the classic paper is Crombie 1955). The same is definitely not found when microwave radar waves are backscattered from a rough sea using normal sizes of illuminated patch (see Wright 1978).

3.3 The limits of Bragg scattering theory for a rough sea and how these lead to the concept of a primary scene element

There is a well-known oceanographic theorem due to O M Phillips (1958) which states that when a gravity wave system is in equilibrium with the local wind, the high-frequency tail of the one-dimensional wave spectrum falls off as frequency^{-5}, or

$$S(\omega) \simeq \alpha\, g^2/\omega^5$$

where ω = 2π • frequency

$S(\omega)$ is the spectral density

g is the acceleration due to gravity

α is a non-dimensional constant usually taken to equal 8.10×10^{-3}

It is not known how far this law extends into the short-wave end of the wave spectrum though some very recent work at IOS (J A Ewing, private communication) indicates that it is valid to at least 4 Hz ($\lambda \simeq 10$ cm) at moderate windspeeds. However, it is not critical for the present argument that it be obeyed exactly, only that the general trend of a rapid decrease in spectral density with decreasing wavelength takes place.

If ζ is the vertical displacement of the water surface, then the mean square displacement $\langle\zeta^2\rangle$ due to components of the wave spectrum with frequencies higher than Ω is $\int_{\Omega}^{\infty} S(\omega)d\omega$, or from the above equation

$$\langle\zeta^2\rangle = \alpha g^2/4\Omega^4$$

The wavelength λ_1 corresponding to Ω is given by $\lambda_1 = 2\pi g/\Omega^2$

$$\therefore \qquad \langle \zeta^2 \rangle = \alpha \lambda_1^2/(4\pi)^2$$

Or the rms displacement ζ_{rms} is given by

$$\zeta_{rms} = \alpha^{\frac{1}{2}} \lambda_1/4\pi \cong 7.10 \times 10^{-3} \lambda_1 \qquad (3)$$

This is the rms displacement due to components of the wave spectrum with wavelengths less than λ_1.

Without it being necessary to consider precisely how the various wavelength components in the sea wave spectrum contribute to the departure of a small area from a plane surface, this shows that such departures are proportional to the linear size of the area. Thus, if a small enough sub-cell of the sea surface is chosen, it will be possible to apply linear perturbation theory to it, and hence use the concept of Bragg scattering within it.

Consider, for example, the case of the Seasat SAR.

If the criterion for small roughness is that $\zeta_{rms} < \lambda_R/2\pi$, then for Seasat we require that $\zeta_{rms} < 3.7$ cm. Again without worrying about the precise contribution of various wavelengths to the roughness, equation (3) shows that this criterion will be satisfied by a square sub-cell of size, say, 2 m, and the Bragg resonant condition can be applied within it even though it contains only about 6 Bragg wavelengths.

Such sub-cells represent the primary scene elements, and it is now possible to make an approximate estimate of their decorrelation time.

3.4 The decorrelation time of a primary scene element

The processes by which energy is fed into and extracted from short wavelength ripples are not well-enough understood to allow us to calculate decorrelation times with confidence. Measurements are difficult and existing data usually refers to patch sizes too big to be directly relevant to the present problem, though some indirect inferences can be made. However, the writer believes that the following calculations are probably sufficiently valid to give a guide, and it will be seen later in the paper that so long as the order of magnitude deduced is correct, the precise results are not critical.

The arguments become clearer if related to a specific radar and the Seasat SAR will be used, but again, they are generally applicable in principle.

The first order Bragg resonant wavelength for the Seasat SAR was approximately 34 cm.

The relevant properties of a water wave of this wavelength are

Phase velocity 0.72 m/s

Group velocity 0.36 m/s

Decay-time to half amplitude due to viscosity 15.7 min

Thus, apart from a significant Doppler shift due to the phase velocity (see section 5.8 for the effects of this) it is clear that the pattern of the Bragg resonant waves within a 2 m sub-cell will change on a timescale of considerably greater than 1 s.

The sub-cell will also be tilted by the longer waves present, and equation (2) shows that this alters the Bragg resonant wavelength. When horizontal, a 2 m patch contains 6 Bragg waves. If these waves were "frozen" and the surface tilted, resonance with them would be completely lost when the new Bragg wavelength has either 5 or 7 waves in the patch.

For Seasat SAR we have

Horizontal patch $\lambda_B = (23.5/2)/\sin 20.5^o = 33.6$ cm

For $\lambda_B = 33.6$ cm x $6/7$, $\theta_i = 24.1^o$

For $\lambda_B = 33.6$ cm x $6/5$, $\theta_i = 16.9^o$

Tucker (1980) for a different purpose defines a roughness parameter R which is the mean-square wave slope due to spectral components with wavelengths greater than approximately 6 m, which happens to give a value approximately correct for the present purpose. He calculates it as a function of wind speed for both the Pierson-Moskowitz formula and from measured spectra. Typical values at moderate wind speeds (~ 10 m/s) are in the region of 10^{-2}, giving rms slopes of approximately 6^o. It is not worth going into full spectral calculations of the rate of change of slope, but to get a typical value we can take the dominant wave period of approximately 6.3 s corresponding to a 10 m/s wind, giving a corresponding $\omega = 1\ s^{-1}$ and a typical rate of change of slope of approximately 6^o/s. Thus, typical decorrelation times due to tilting of the patch are likely to be of the order of 0.5 s.

It might have been better compromise to use a patch 1 m across. This would decorrelate due to tilt comparatively slowly and infrequently and decorrelation due to group velocity etc would still be slower than 1 s. However, this is not really critical, since it has been demonstrated that there is in principle a small patch size which decorrelates in a time which is comparable with or longer than the SAR integration time, and other effects to be described below actually result in a decorrelation of the resolution cell on a much faster timescale, so that little final error is involved in assuming the primary scene element to be a constant target during integration.

4. THE COMPOSITION OF A RESOLUTION CELL

4.1 General concepts

Consider first a real aperture side-looking radar looking at a boulder-strewn field. Because of the radar's finite beam-width and pulse-length, the signal received at any instant is the sum of the signals from many boulders in the field of view. It is in fact a weighted sum of the target strengths of the boulders, the amplitude of the weighting function generally decreasing away from the centre of the illuminated patch. The nominal resolution is usually defined as the 6 db width of this function in range and azimuth.

The sum takes account of the amplitude and phase of the returns from the individual targets. Since the phase in particular is random, the way the individual boulder target strengths add is the well-known "random walk" problem, and the resultant amplitude follows a Rayleigh probability distribution. The corresponding distribution of the measured back-scattering cross-section σ (proportional to $|\text{amplitude}|^2$) is negative exponential. The mean value of the distribution of σ (called its expected value σ_e) is the sum of the expected values of the cross-sections of all the elements which compose it.

The random variation of the return from pixel to pixel is termed "speckle", and this re-randomises quickly as the radar moves. The Seasat SAR, for example, obtained 4 independent samples (or "looks") within its nominal resolution cell. These looks are averaged incoherently in the detector to obtain some reduction in the speckle background. This does not affect the arguments presented below.

The important point to note for the present purpose is that in terms of the concepts developed in this paper, the radar returns from the primary scene elements pass through the aperture synthesis process separately (see section 2.2). Each is offset azimuthally according to equation 1 and all those finishing up in a particular resolution cell are added in the way

outlined above. The expected value σ_e of the backscattering cross-section measured at the centre of this resolution cell is the sum of the expected backscattering cross-sections of all the primary scene elements.

4.2 The relationships between Doppler spectra, decorrelation time and azimuthal offsets

The purpose of this section is to discuss briefly the relationship between the different ways in which the problem has been approached by different workers.

If the targets referred to above were each moving independently in the range direction, each would produce its own Doppler shift in the returned signals. For the case of waves, these shifts can be seen when a small area of the sea-surface is illuminated with a CW radar, (Keller, Plant and Valenzuela, in press). When many targets moving at random are within the resolution cell of the radar, they will produce a band of frequencies. If the width of this is δf, a well-known theorem states that the decorrelation time $\tau_D \simeq 1/\delta f$. This relationship is not affected by a superposed Doppler shift of the resolution cell as a whole. Raney (1980), for example, has worked with decorrelation times.

In the case of waves, as the size of the resolution cell is increased the velocity differences within it will be increased (see equation 14 and figure 4) so that decorrelation time decreases. The effect is shown qualitatively in figure 1. The upper limit of decorrelation time depends on various factors, including the decorrelation time of the primary scattering elements as discussed in section 3.4. It is in effect argued there that this significantly affects only the left-hand half of figure 1, whereas the resolution cell of a SAR is typically 100 Bragg wavelengths or more across.

For present purposes it is convenient to work in terms of the azimuthal offsets due to the range component of velocity (equation 1). since this leads directly to an expression for the resultant azimuthal smearing. In the SAR processor, these offsets actually result from the Doppler shifts due to the velocities.

One can transform any representation into any other. For example, if the time-dependence of the decorrelation is known it can be converted to the equivalent frequency spectrum by a Fourier transform. Each component of this spectrum is indistinguishable from a Doppler shift, which therefore produces an azimuthal offset after processing in the SAR.

4.3 Separation of speckle and wave modulation effects

The speckle statistics are modified by the wave modulation. However, for radars with steep angles of incidence (which is the type considered in the present paper) the wave modulation is usually comparatively small and to first order it is possible to consider the overall speckle statistics of the image as being unaffected by the waves: this assumption is made in most published work on wave visibility in SARs. Equally, when dealing with the statistical properties of the wave modulation (in particular its spectrum) we need consider only the way the waves modulate σ_e, the expected value of the backscatter cross-section (ie the mean of its probability distribution).

Thus, to first order, the spectrum of the image consists of the spectrum of the wave modulation superposed on the spectrum of the speckle, which is that of the impulse response function.

4.4 Separation of the effects of small scale and large scale motions

We shall temporarily consider the image as being divided into discrete resolution cells (that is, a sharp-edged point-target impulse response function).

Taking account of the linear superposition of velocity effects discussed in section 2.2, the velocity offset process can be considered in two stages as shown in figure 3. In the first, the primary scene elements within a resolution cell all move the same distance azimuthally due to the mean range component of velocity of the cell. In the second, they scatter due to the relative motions within the cell.

The first process can be a mechanism for imaging low-amplitude swell. This is shown diagramatically in figure 4 and is known as "Velocity bunching". The within-cell motions will be shown to produce a very significant smearing of the spectrum, removing components with short wavelengths in the azimuthal direction.

5. THE EFFECTS OF SEA-SURFACE MOTION ON THE IMAGE

5.1 Summary of the position reached so far in this paper

The imaging process can be considered as a series of independent steps.

(a) The primary scattered field can be considered as that produced by the primary scattering elements whose target strengths are constant during the SAR integration period. The expected value of the target strengths of these elements is modulated by factors such as wave slope and hydrodynamic modulation to give the primary scattered field.

(b) This field is then operated on by the azimuthal offsets caused by the range velocity component of the resolution cells as a whole, which may produce further wave modulation by the velocity bunching effect.

(c) This field is then smeared azimuthally by the within-cell motion effects.

5.2 Separation of motion scales in terms of the wave spectrum and its application to numerical simulation

The theorem allowing the independent superposition of the effects of velocity components (section 2.2) can also be applied to velocities due to different parts of the wave spectrum. This is in many ways a more convenient division than the spatial one used above, since with the first order assumption that waves are a stationary random Gaussian process, the various spectral components are uncorrelated. Thus, if, for example, we divide the spectrum into two parts at a frequency above which none of the components are imaged, the azimuthal offsets due to the high frequency components will be uncorrelated with the imaged components and can therefore be treated as random.

Such a concept has a direct application in numerical simulation of SAR imaging. The need for this arises because the velocity-bunching modulation can be considered as a linear problem only for long low swells. The effect of large amplitudes becomes a difficult non-linear problem for which no analytic solution is yet available (this subject is discussed by Alpers et al 1981 and Raney 1981). Thus, an understanding of the effects can only be achieved by numerical simulation of the radar imaging process using a variety of typical wave spectra as input (Hasselmann and Alpers, private communication). For this it is economically important to use the coarsest possible grid, particularly for two-dimensional simulation, and since all frequencies in the input spectrum above the corresponding Nyquist frequency have to be removed, it would be desirable to be able to treat the effects of higher frequencies in some other way.

If the grid points are placed at the centres of the resolution cells, the Nyquist frequency corresponds to a wavelength $\lambda_N = 2\rho$, which is the criterion usually used for the limit of wavelength resolution of the radar.

The theory will now be given using this division, and finally, in section 5.6 the arguments will be extended to see what more general conclusions can be drawn.

5.3 The effect of small-scale velocities: the basic theorem

Define the image intensity of a particular scene as

$$s(x,y) = \frac{\sigma(x,y) - \sigma_o}{\sigma_o}$$

where σ_o is the ensemble average of $\sigma(x,y)$ over the scene and x is the azimuthal direction.

s(x,y) over a large rectangular scene can be considered as the sum of sinusoidal harmonics (the Fourier theorem).

$$s(x,y) = \sum_l \sum_m A_{lm} \exp i\{k_l x + k_m y\} \qquad (4)$$

where A_{lm} is the complex amplitude of that harmonic which has l complete wavelengths in the x dimension of the scene and m complete wavelengths in the y dimension, and k_l and k_m are the corresponding wave numbers.

The next point can be made most clearly by temporarily considering s(x,y) as being an actual digital radar image, so that s(p,q) is available for the pixel in the pth column and qth row, the unit of distance being taken as the pixel spacing. Then the Fourier transform of the image is

$$A_{lm} = \frac{1}{N} \sum_p \sum_q s(p,q) \exp -i\{k_l p + k_m q\} \qquad (5)$$

where N = p q

This equation shows that the amplitude of a given frequency component is a weighted average of all the pixel intensities in the image. In a typical transform (see the appendix) there are about 10^5 pixels, but the final spectral estimates may be based on the average of the transforms of a number of such scenes, is that the number of pixels finally involved is typically of the order of 10^6.

Thus, if we are considering effects which are random with respect to the l, m^{th} harmonic (that is, uncorrelated with it) and whose space scale is comparable with a pixel dimension, we can treat them on a probability basis.

Suppose now that equations 4 and 5 refer to a primary scattered field, and consider notionally that it consists of small pixels with a spacing of δ in both dimension, each pixel being due to a primary scattering element. If the azimuthal offset due to range velocity is χ, assumed to be generally fairly large compared with δ, the proportion of pixels which are offset in such a way that their new centres fall within the pixel which has its centre n pixels away (along the x axis) from the original position is $p(\chi_n)\ \delta$, where $p(\chi)$ is the probability density function of χ, and $\chi_n = n\delta$.

The offsets we are concerned with here are uncorrelated with the longer-wave components (this statement is justified below). Therefore, so far as these long waves are concerned this particular set of pixels is a random selection from the primary scattered field. It therefore has the same Fourier transform, but shifted a distance χ_n along the x axis. If $\Delta A'_{lm}$ is its contribution to A'_{lm}, a harmonic of the SAR-processed field, then

$$\Delta A'_{lm} = p(\chi_n)\delta\frac{1}{N}\sum_p\sum_q s(p,q)\ \text{exp-i}\{k_l\ (x + \chi_n) + k_m y\}$$

$$= p(\chi_n)\delta\ \{\text{exp-i}\ k_l\ \chi_n\}\ \ A_{lm}$$

Since δ is the interval of χ corresponding to this contribution to A'_{lm} this can be converted to an integral

$$A'_{lm} \rightarrow A_{lm}\int_{-\infty}^{\infty} p(\chi)\{\text{exp-i}\ k_l\ \chi\}\ d\chi$$

Or, using the symbol k_x instead of k_l, the amplitude response function of the aperture synthesis process is

$$R(k_x) = \int_{-\infty}^{\infty} p(\chi)\{\text{exp-i}\ k_x\ \chi\}\ d\chi \qquad (6)$$

Before evaluating this integral it is necessary to justify the statement that χ is uncorrelated with the longer wave components. In this section we are considering only the effect of the motions due to that part of the wave spectrum with wavelengths below 2 ρ, on the imaging of components of

the wave spectrum with wavelengths greater than 2 ρ. As pointed out above, if first-order wave theory is assumed, these regions of the spectrum are uncorrelated.

It is also necessary to state that the spatial correlation of the velocity field due to the short wavelength part of the spectrum falls off on a scale of the order of ρ. This follows from the spatial equivalent of the time-domain law quoted in section 4.2, plus an oceanographic knowledge of the shape of the spectrum in this region (see below). Thus, there is a very large number of effectively independent offsets in the scene, as discussed earlier in this section.

5.4 The evaluation of the response function

The standard first-order model of wind generated waves shows that the surface elevation $\zeta(t)$ above a fixed point on the seabed has a random Gaussian probability distribution (see, for example, Kinsman 1965 section 7.4). This arises because the sea-surface can be considered as the random superposition of many sinusoidal components travelling independently. The particle velocities can also be taken as superposing independently, and since the component of the particle velocity in a fixed direction due to a component wavetrain varies sinusoidally in time, the sum of the particle velocities in a fixed direction also has a Gaussian probability distribution. Because the process is ergodic, this is true of the time-variation of particle velocity at a fixed point, and of the spatial variation at a fixed time.

The relevant particle velocity is the range component v_r.

Using equation 1 gives the probability density function of the resulting azimuthal offset:

$$p(\chi) = \frac{1}{\nu\sqrt{2\pi}} \exp(-\chi^2/2\nu^2) \qquad (7)$$

where $$\nu^2 = \langle\chi^2\rangle = (R_s/V_s)^2 \langle v_r^2\rangle \qquad (8)$$

When considering the backscattering from the sea surface the targets are the primary scene elements discussed in section 3, and superimposed on the wave particle velocities will be the phase velocity of the Bragg resonant wave. The effect of this is discussed in section 5.8. In order to simplify the present discussion we shall consider here that we are concerned only with either the approach component of the Bragg waves or the receding component, and not with a mixture of both. The effect will then be to add a constant velocity, and thus a constant offset, to the whole radar scene, and this can be neglected.

Using equations 6 and 7 gives

$$R(k_x) = \frac{1}{v\sqrt{2\pi}} \int_{-\infty}^{\infty} \exp -i(k_x \chi) \exp(-\chi^2/2v^2)\, d\chi$$

This integral can be looked up in standard works of reference, giving

$$R(k_x) = \exp(-k_x{}^2 v^2/2) \qquad (9)$$

Thus, the effect of the short wavelength components of range velocity is equivalent to a filter removing the shorter azimuthal components of wavelength (higher wavenumber components). The 3 db response is at $\lambda_x = 2\pi/k_x = 7.55v$ and the half amplitude response is at $\lambda_x = 5.33v$.

Many digitally-computed spectra from Seasat images show what appears to be azimuthal filtering of this type (figures 5 and 6).

5.5 Calculation of the filter assuming a Pierson-Moskowitz wave spectrum

If one knew the directional spectrum it would be possible to compute the rms range component of velocity from it. However, for satellite-borne SARs with a steep angle of incidence a major simplification is possible.

In a simple long-crested periodic wave train of amplitude a and frequency f in deep water, the water particles travel in circular orbits

whose planes are in the direction of propagation of the waves. In such a wave travelling in the range direction, the plane of the circle contains the radar range direction and the radar would see an rms range velocity of $\sqrt{2\pi}af$. If travelling azimuthally the range component of velocity would be reduced by cos θ_i, where θ_i is the angle of incidence of the radar beam and for other directions by a factor between cos θ_i and 1. For the Seasat nominal θ_i of 20.5^{o}, cos θ_i = 0.972. Thus, there is less than 3% error involved in assuming that the rms range component of velocity is $\sqrt{2\pi}af$ independent of direction of travel. Using the assumption that the sea can be represented by a spectrum of component wave trains travelling independently then leads to

$$\langle v_r^2 \rangle \simeq \int_{\Omega_1}^{\Omega_2} \omega^2 \, 2(\omega) \quad d\omega \tag{10}$$

where $\omega = 2\pi f$

$S(\omega)$ is the one-dimensional spectral density of surface elevation

Ω_1 and Ω_2 are the relevant limits of integration, to be discussed later.

A commonly-used formula for the one-dimensional spectrum in a fully arisen sea is the Pierson-Moskowitz spectrum (see, for example, Silvester 1974).

$$S(\omega) = \frac{\alpha g^2}{\omega^5} \exp\{-\beta(g/U\omega)^4\} \tag{11}$$

where $\alpha = 8.10 \times 10^{-3}$)
$\beta = 0.74$) dimensionless constants

U = wind speed at a height of 19.5 m

Putting this into equation 10 leads to

$$\langle v_r^2 \rangle = \int_{\Omega_1}^{\Omega_2} \alpha \, g^2 \, \omega^{-3} \exp\{-\beta/g/U\omega)^4\} \, d\omega$$

$$= \frac{\alpha\sqrt{\pi}}{4\beta^{\frac{1}{2}}} U^2 \{\text{erf } \beta^{\frac{1}{2}}(g/U\omega)^2\}_{\Omega_2}^{\Omega_1}$$

where erf is the error function, tabulated in standard works.

Using the deep water dispersion relationship $\omega^2 = 2\pi g/\lambda$ where λ is the wavelength gives

$$\langle v_r^2 \rangle = \frac{\alpha\sqrt{\pi}}{4\beta^{\frac{1}{2}}} U^2 \left\{\text{erf } \frac{g\beta^{\frac{1}{2}}}{2\pi} \cdot \frac{\lambda}{U^2}\right\}_{\lambda_2}^{\lambda_1} \tag{12}$$

Putting in the numerical values for the constants (using g - 9.81 m s^{-2})

$$\langle v_r^2 \rangle = 4.17 \times 10^{-3} U^2 \left\{\text{erf } 1.344 \frac{\lambda}{U^2}\right\}_{\lambda_2}^{\lambda_1} \tag{13}$$

(λ in m, U in m/s)

$4.17 \times 10^{-3} U^2 \{\text{erf } 1.344 \lambda/U^2\}$ is plotted against λ with U as a parameter in figure 4 and the limits of integration can now be considered.

It will be seen that the function drops off rapidly at small wavelengths, and thus the lower limit of integration is not critical. The issue of what is the correct lower limit can therefore be avoided by integrating from zero, knowing that if, for example, it should actually be 1 m, as it was argued in section 3.4 might be appropriate for the Seasat SAR, the error introduced in $\langle v_r^2 \rangle$ would be less than 5%, and typically more like 2%, with any reasonable wind speed.

Taking the upper limit as $\lambda_2 = 2\rho$ (see section 5.2) then gives

$$\langle v_r^2 \rangle \simeq 4.17 \times 10^{-3} U^2 \text{ erf } \{1.344 \frac{2\rho}{U^2}\} \tag{14}$$

It is worth noting that since the above calculation deals with the short wavelength end of the spectrum, in most circumstances the wave energy will be characteristic of the local wind, whereas for longer waves the energy is often swell from a distant storm.

Using equation 8, the rms azimuthal offset ν is given by

$$\nu^2 = 4.17 \times 10^{-3} (R_s/V_s)^2 U^2 \text{ erf } \{1.344 \frac{2\rho}{U^2}\} \tag{15}$$

$$\rightarrow 1.265 \times 10^{-2} (R_s/V_s)^2 \rho \qquad \text{for } U^2 >> g\rho \text{ (see equation 12)}$$

This asymptote corresponds to the line marked "U = ∞" in figure 4. These relationships can be put into equation 9 to give the azimuthal filter function.

5.6 More general consideration of the effect

There will be occasions when a natural division occurs in the wave spectrum at the resolution limit. Examination of the Pierson-Moskowitz equation for a fully arisen sea (equation 11) shows that there is negligible energy in wavelength components longer than approximately $\lambda = 1.5\ U^2$ (cgs units). For Seasat, for example, this implies that for winds less than about 6.5 m/s, none of the locally-generated wave energy can be imaged even within the nominal resolution. There may, however, be longer swell present. In general the rms velocity component due to the swell is likely to be rather small, so that an approximate value for the azimuthal filter can be calculated using the locally-generated wave energy alone. There is a Seasat image corresponding to such a case for which some relevant surface observations are available, and this is discussed in section 5.7.

In the more general case, equation 15 inserted into equation 9 will give a minimum value (in terms of wavelength) for the azimuthal cut-off for given local winds, and this is significant because in nearly all cases it will represent a considerable degradation of the nominal resolution.

If one were examining the effect on a known directional wave spectrum, it would be possible to iterate this process, each iteration including the rms velocity due to components cut out of the imaging by the previous calculation. This would still only give a minimum value, since it seems likely that some imaged components contribute to the smearing, but the author cannot at present see how to treat the complete problem by analytical means.

5.7 An example from Seasat

At 0650 hours on 19 August 1978 Seasat produced an image of the sea surface at 60^{o} 11" N and 6^{o} 41' W. The image and its spectrum are shown in figures 5 and 6. At 0800 hours the Natural Environment Research Council's research vessel JOHN MURRAY was at 60^{o} 40' N and 8^{o} oo' W and took wind speed measurement of 6.5 m/s from 170^{o}T and a significant waveheight measurement of approximately 5 m. The ship was under way at the time so that the Shipborne Wave Recorder gave no wave period measurement, but the visual observer estimated a swell of 10 s period with a height of about 4.5 m coming from 240^{o}T and a local wind sea of about 7 s period and a height of about 2 m coming from 200^{o}T. A cold front was passing the area at the time so the wind may have been slightly variable, but the isobar spacing was about the same on both sides of the front and uniform over quite a large area of ocean in the vicinity.

IOS also had a Waverider operating in 100 m depth of water at 60^{o} 10' N, 2^{o} 44' W (west of the Shetland Islands). Due to Citizens Band radio interference only intermittent records were being obtained, but good quality records were obtained for 1741 hours on 18 August and 1741 hours on 19 August. The spectra from these are shown in figure 7 and show clearly the band of swell at approximately 10 s period. The values of Hs are considerably lower than the 5 m recorded at the JOHN MURRAY, but with southerly winds this site has limited fetch.

Using the JOHN MURRAY wind of 6.5 m/s and a resolution of $\rho = 30$ m, equation 14 gives $\langle v_r^2 \rangle = 0.1758\ (m/s)^2$.

The value $R_s/V_s = 115$ for Seasat then gives $\nu = 48$ m or a 3 db azimuthal cut-off at a wavelength of 364 m, or a half amplitude cut-off at a wavelength of 257 m. (It can be shown that with a satellite travelling in a curved orbit the relevant velocity is that in orbit, not that over the ground.)

The image spectrum will be the product of the spectrum of the primary scattered field multiplied by the filter function, but if we make the assumption that, apart from the long-wave swell peak, the primary spectrum does not vary with direction, then figure 6 shows a fairly constant width azimuthally with a 3 db cut-off of approximately 380 m and a 6 db cut-off of approximately 250 m, which is good agreement in the circumstances. (Note that the dominant wavelength of the locally-generated sea would have been about 30 m for a 6.5 m/s wind.)

Apart from the fact that we have some ground truth for this particular example, it is a relatively simple one since the modest local wind means that most of the mean-square particle velocity is contributed by components with wavelengths of less than 60 m (about 2/3 in the case of the South Uist spectra shown in figure 7).

5.8 The effect of the phase velocity of the Bragg waves

The phase velocity of a surface wave increases with wavelength except in the capillary wave region. Some examples are:

Wavelength m	Phase velocity m/s
1.0	1.249
0.25	0.626
0.10	0.401
0.04	0.272
0.02	0.233
0.01	0.248

Assuming that the waves are travelling horizontally in the range direction on an otherwise calm sea, the range component of the velocity is the above value multiplied by $\sin \theta_i$. For Seasat, $\sin \theta_i \simeq 0.35$, so the phase velocity of the Bragg wave is 0.725 m/s, giving a range component of 0.254 m/s, corresponding to an azimuthal offset of approximately 33 m.

The Bragg wave can be travelling towards or away from the radar. If only one of these possible components is present, the whole scene will be offset by 33 m which is unimportant. If, however it happens that an azimuthal wind is blowing so that both components are present in roughly equal amplitudes, two images will be produced offset from one another by 66 m. This would produce cancellation of components in the spectrum with azimuthal wavelengths of approximately 132 m (Rotherham in press). However, as calculated above, such components will already have been removed by the short wavelength smearing in all except the calmest seas, so such a minimum in the spectrum is only likely to be observed in very unusual circumstances.

For shorter wavelength radars with slower Bragg waves, the effect will be less, of course.

6. CONCLUSIONS

Using arguments based on the way the internal roughness of a patch of the sea surface decreases with its size, it has been shown that Bragg resonant scattering can be applied to a patch of sea surface a few wavelengths across. The target strength of such a patch can be regarded as approximately constant for a SAR integration time: certainly for a time much longer than the decorrelation time of a resolution cell.

Since the aperture synthesis process is linear, each of these small patches, called "Primary scattering elements" can be carried through the process independently, and are offset azimuthally according to their local range components of velocity.

The linearity of this process also means that the offsets caused by velocities arising from the long and from the short wavelength parts of the spectrum can be treated independently. A convenient dividing line corresponds to the resolution limit of the radar. The effect of long wavelengths can be modelled by numerical simulation, that of short wavelengths can be treated

statistically. If the computations are carried out in this order, the short wavelengths produce an azimuthal smearing which has the effect of a filter which in terms of wave number is Gaussian low-pass, acting on the final image. For Seasat SAR in moderate seas the cut-off wavelength is several hundred meters.

Several Seasat images of waves show effects which can be interpreted in this way.

This type of effect sets an important limitation on the utility of a satellite-borne SAR for measuring waves.

REFERENCES

ALPERS N R, ROSS D B and RUFENACH C L, 1981. On the detectability of ocean surface waves by real and synthetic aperture radar. J Geophysical Research Vol 86, No C7, pp 6481-6498.

BARRICK D E, 1972. First order theory and analysis of MF/HF/VFH scatter from the sea. IEEE Trans Antennas & Propagation Vol AP-20, pp 2-10.

BASS F G, FUKS I M, KALMYKOV A E, OSTROVSKY I E and ROSENBERG A G, 1968. Very high frequency radiowave scattering by a disturbed sea surface. IEEE Trans. AP-16, pp 554-568.

CROMBIE D D, 1955. Doppler spectrum of sea echo at 13.56 Mc/s. Nature, Vol 175, pp 681-682.

JORDAN R L, 1980. The Seasat-A synthetic-aperture radar system. IEEE Journal of Oceanic Engineering, Vol OE-5, No 2, pp 154-163.

KELLER W C, PLANT W J and VALENZUELA G R, (in press). Observation of breaking ocean waves with coherent microwave radar. Proc. Conference on Wave Dynamics and Radio Probing of the Ocean, Miami, 13-20 May 1981. To be published by Plenum Press.

KINSMAN B (1965). Wind waves. Published by Prentice-Hall, New Jersey.

PHILLIPS O M, 1958. The equilibrium range in the spectrum of wind-generated ocean waves. J Fluid Mechanics, Vol 4, pp 426-434.

RANEY R K, 1980. SAR processing of partially coherent phenomena. Int J Remote Sensing Vol 1, pp 29-51

RANEY R K, 1981. Wave orbital velocity fade and SAR response to azimuthal waves. Journal of Oceanic Engineering, Vol OE-6, No 4, pp 140-146.

ROTHERHAM S (in press). Theory of ocean wave imagery. "Seasat over Europe". Ed T D Allan, Proc. Conference in London 14-16 April 1982. to be published by Horwood, Chichester, England.

SILVESTER R, 1974. Coastal Engineering, Elsevier, Amsterdam, 457 pp.

TOMIYASU K, 1978. Tutorial review of synthetic-aperture radar (SAR) with applications to imaging the ocean surface. Proc IEEE Vol 66, pp 563-583.

TUCKER M J, 1980. The importance of oceanography to the offshore oil industry. Proc "Petromar 80", Published by Graham and Trotman Ltd pp 437-452.

WRIGHT J W, 1966. Backscattering from capillary waves with application to sea clutter. IEEE Trans, AP-14, pp 749-754.

WRIGHT J W, 1968. A new model for sea-clutter. IEEE Trans AP-16, pp 217-223.

WRIGHT J W, 1978. Detection of ocean waves by microwave radar: the modulation of short gravity-capillary waves. Boundary Layer Meteorology, Vol 13, pp 87-105.

WRIGHT J W, PLANT W J, KELLER W C and JONES W L, 1980. Ocean wave-radar modulation transfer functions from the West Coast Experiment. Journal Geophysical Research, Vol 85, No C9, pp 4957-4966.

APPENDIX: DETAILS OF THE SAR IMAGE AND ITS FOURIER TRANSFORM (FIGURE 5)

The image data was processed by DFVLR and received as follows:

Orbit	0762
Archive Number	0523
Centre of Scene	approximately 60^{o} 11' N, 6^{o} 41' W
Date recorded	19 August 1978
Number of looks	4
Resolution	25 m
Scale	amplitude of target strength
Pixel spacing	12.5 m
Image size	4050 x 4050 pixels

Figure 5a is a 1024 x 1024 pixel sub-area of the image with coordinates (1256, 1256) to (2279, 2279) in terms of pixel number.

Sixteen regions each 256 x 256 pixels were chosen to be Fourier transformed and the $|\text{amplitude}|^2$ of corresponding harmonics were added. A display of this power spectrum showed too much sampling variability to be readily interpretable, so it was further smoothed by a 4 x 4 running average passed over the data.

The image data from DFVLR was in terms of received signal amplitude, whereas the theory outlined in this paper is in terms of backscattering cross-section, or backscattered power. For a number of reasons it was decided to transform the image as received, but since the wave modulation of the mean backscattered intensity is fairly small, the resultant errors will be second order.

The processing was performed by the Marconi Research Centre under contract to the Natural Environment Research Council.

FIGURE CAPTIONS

Figure 1 Qualitative relationship between patch size (assumed circular or square) and the decorrelation time of the backscattered microwave signal.

Figure 2 Azimuthal offsets due to the range components of the sea surface velocities can be considered in two stages. A is one range cell of the primary scattering field. This is transformed to a notional scattering field B by the velocities of the cells as a whole, and into the final image by adding the effects of within-cell motions.

Figure 3 How "velocity bunching" can image a low swell.

A is a vertical cross-section of the swell showing surface velocities

B is a plan view of one range cell. The scattering due to each resolution cell is moved azimuthally by the aperture synthesis process to give the image C, where the scattering is bunched.

Figure 4 The equation $y = 4.17 \times 10^{-3} U^2 \text{ erf } (1.3444 \frac{\lambda}{U^2})$ against λ for various U (with reference to equation 13 in the text)

Figure 5 A Seasat SAR scene and its Fourier transform, showing the azimuthal filtering effect. The contours are at 2:1 intervals of spectral density. Details are given in the Appendix.

Figure 6 Eight cuts across the spectrum shown in figure 5. The plateaus visible at low spectral density correspond to the resolution intervals of the data. The spike on the spectrum for $k_y = 0.122$ is an artefact of the analyses, and has been deleted from the spectrum shown in figure 5.

Figure 7 Wave spectra for 1741 hours 18 August and 1741 hours 19 August 1978. (Note the different ordinate scales.) The significant waveheights were 2.75 m and 3.21 m respectively.

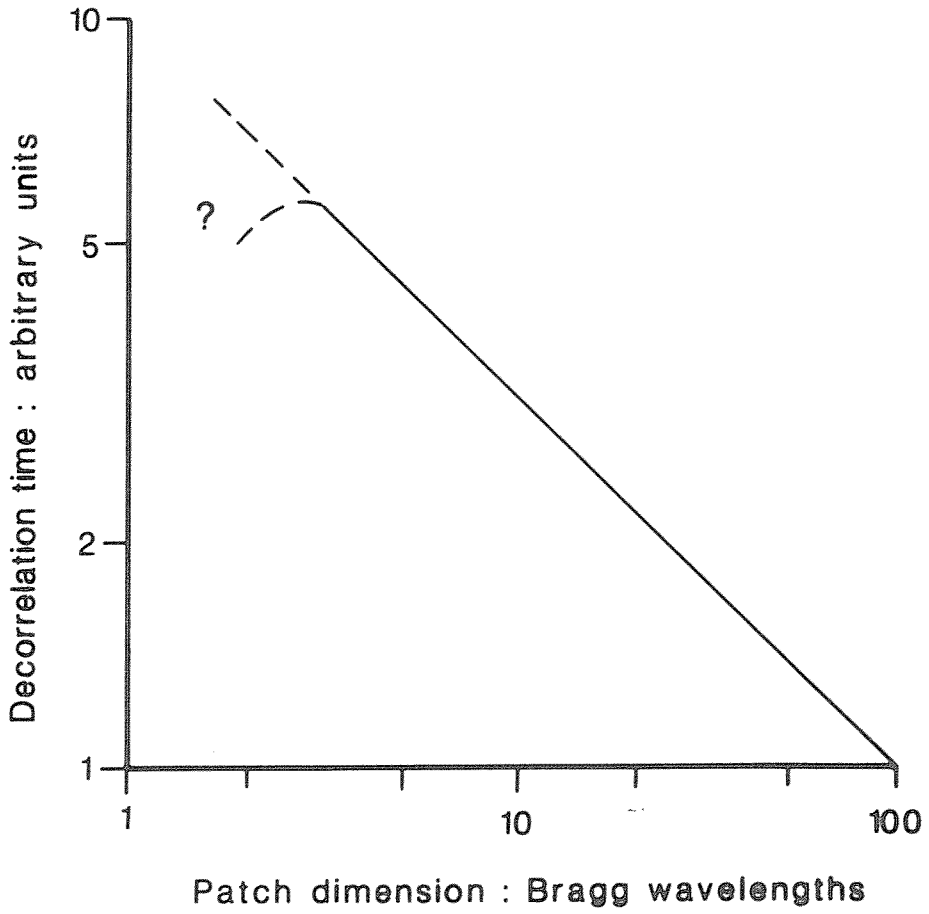

Figure 1 Qualitative relationship between patch size (assumed circular or square) and the decorrelation time of the backscattered microwave signal.

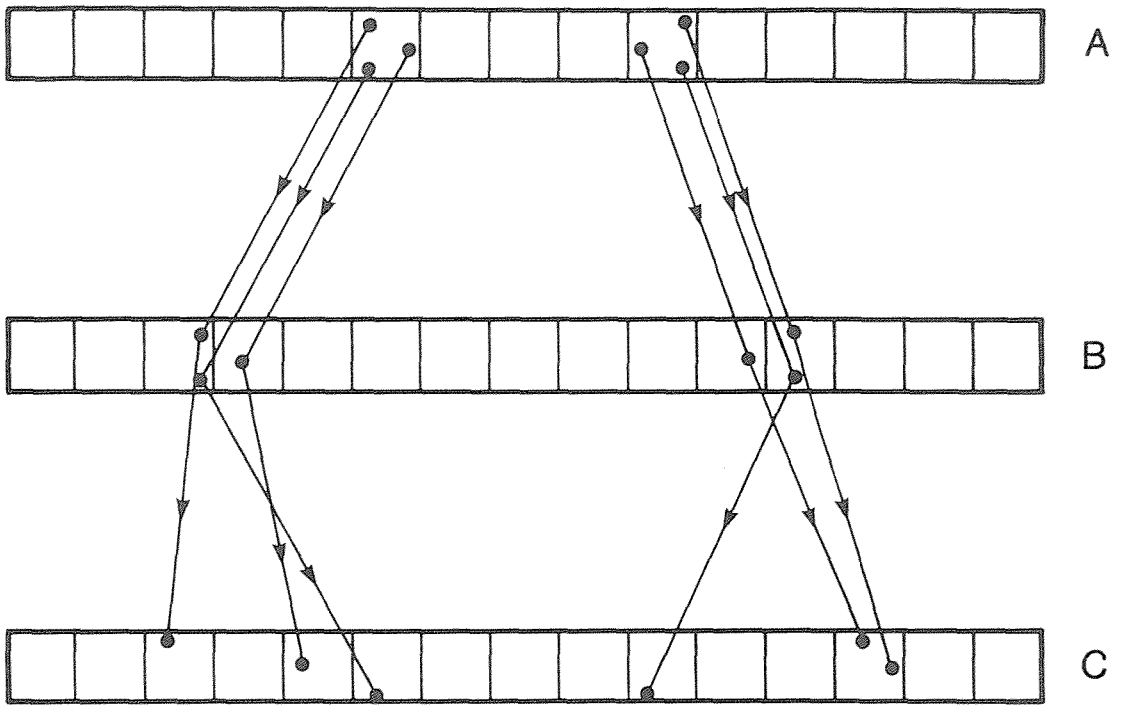

Figure 2 Azimuthal offsets due to the range components of the sea surface velocities can be considered in two stages. A is one range cell of the primary scattering field. This is transformed to a notional scattering field B by the velocities of the cells as a whole, and into the final image by adding the effects of within-cell motions.

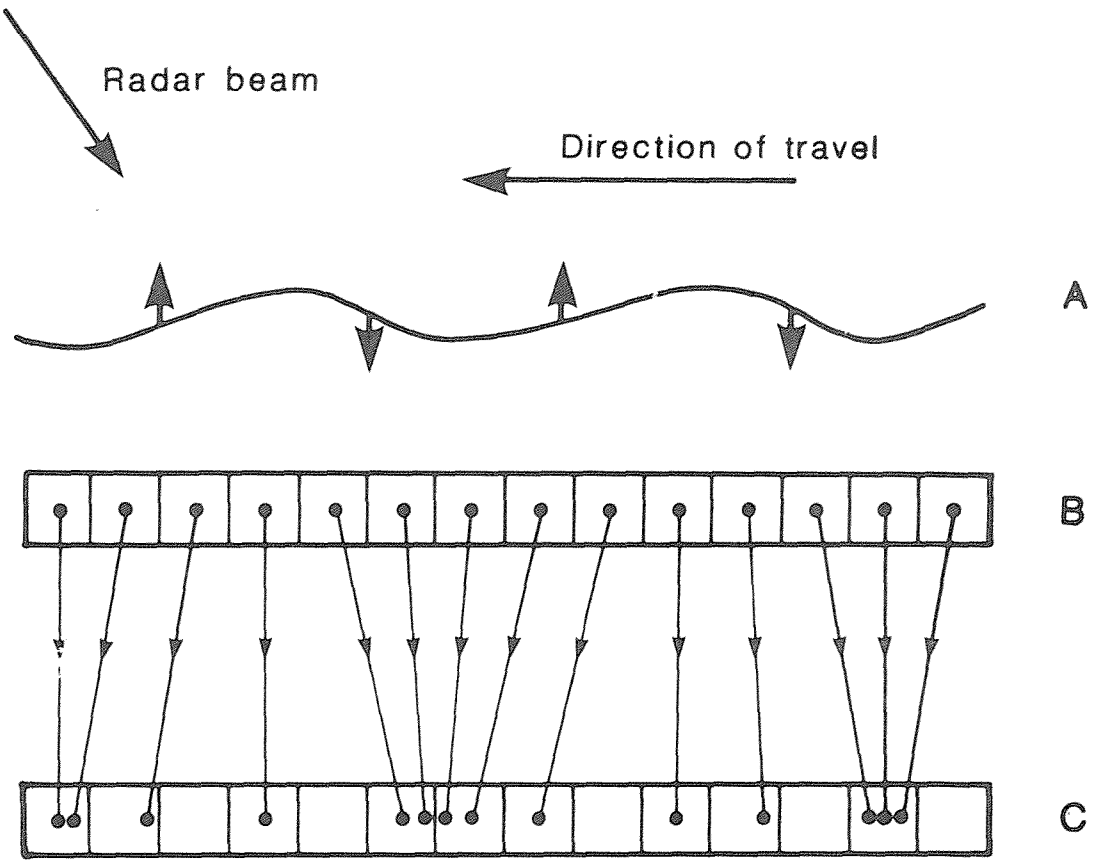

Figure 3 How "velocity bunching" can image a low swell.

A is a vertical cross-section of the swell showing surface velocities

B is a plan view of one range cell. The scattering due to each resolution cell is moved azimuthally by the aperture synthesis process to give the image C, where the scattering is bunched.

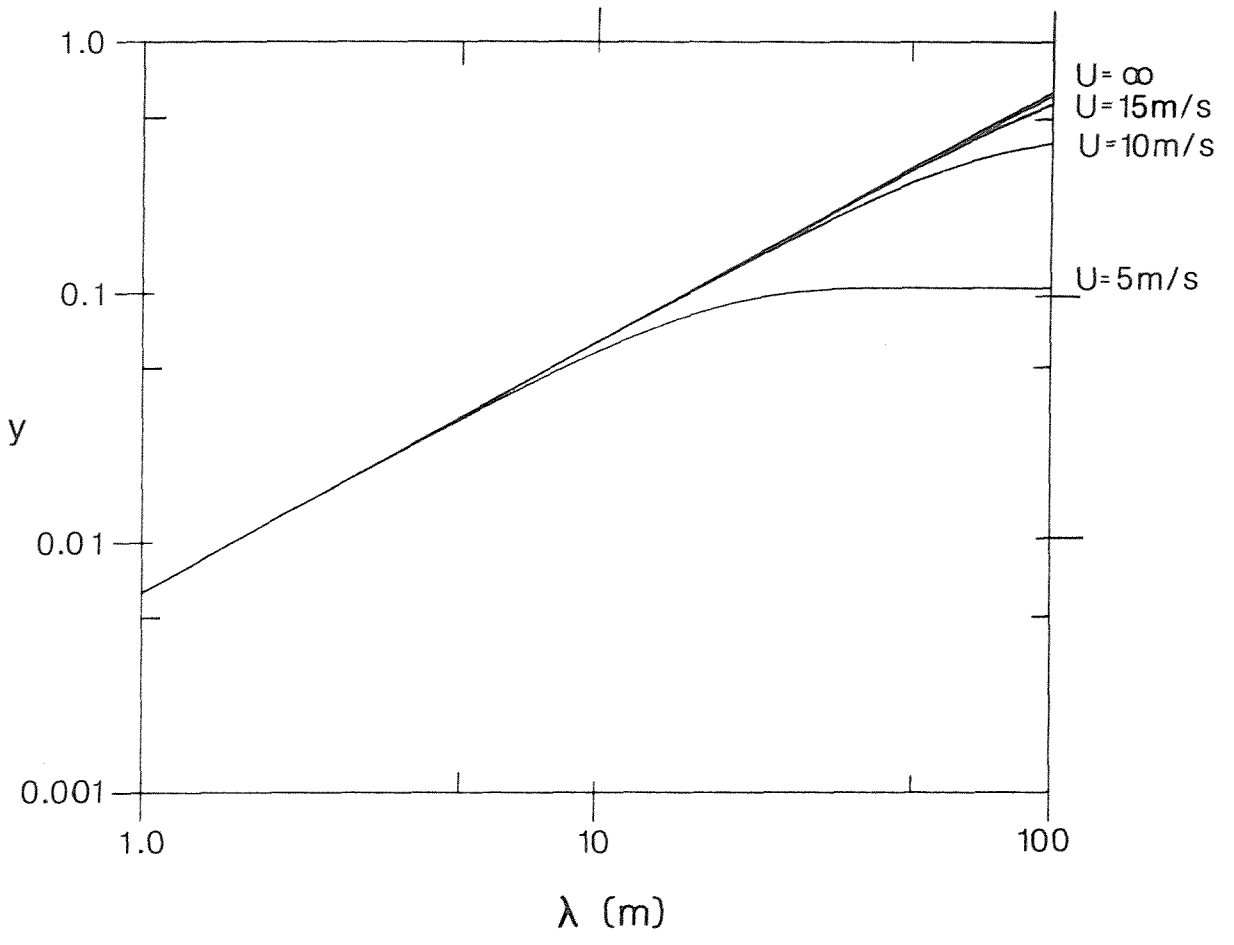

Figure 4 The equation $y = 4.17 \times 10^{-3} U^2 \text{ erf } (1.3444 \frac{\lambda}{U^2})$ against λ for various U (with reference to equation 13 in the text)

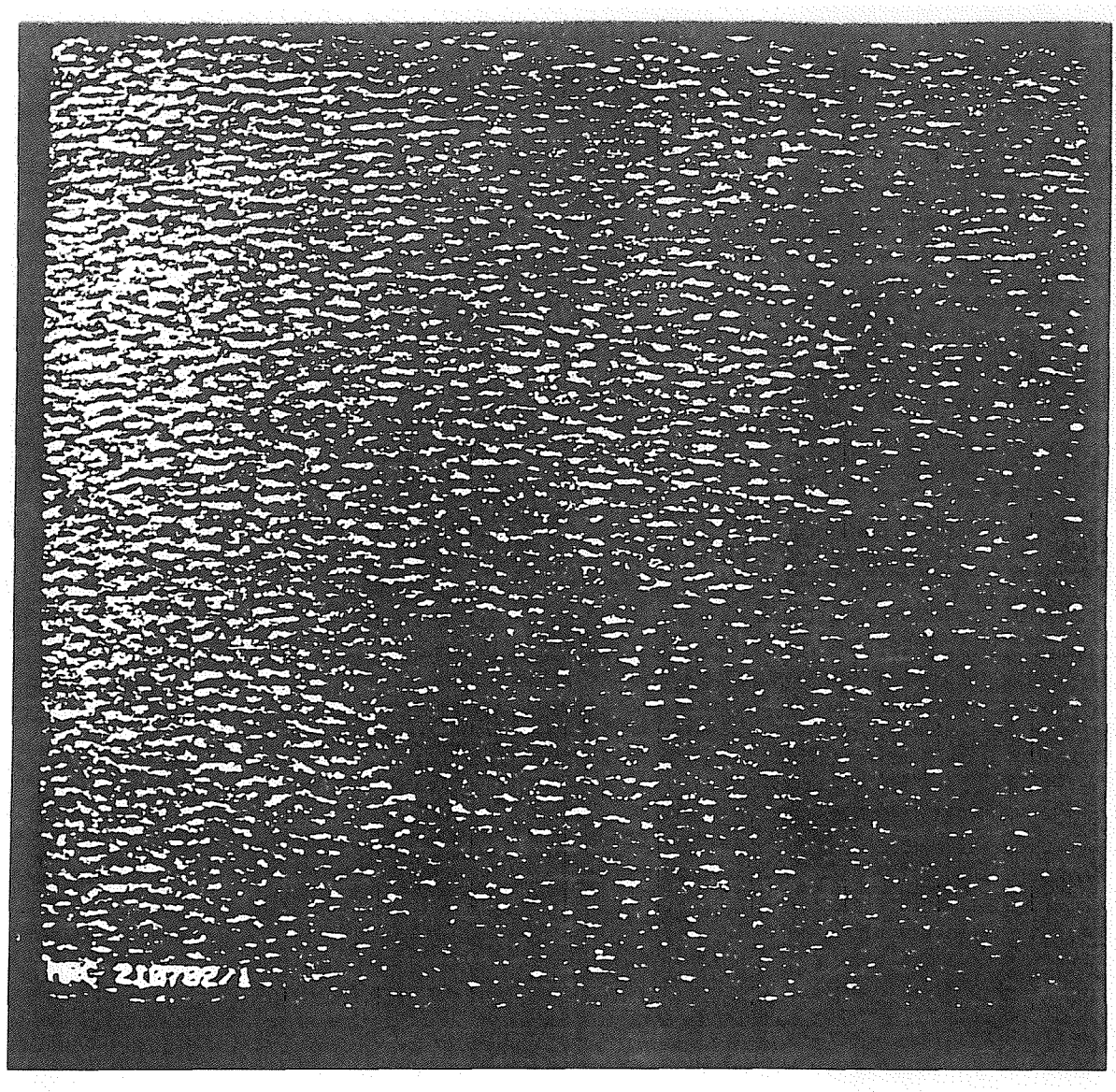

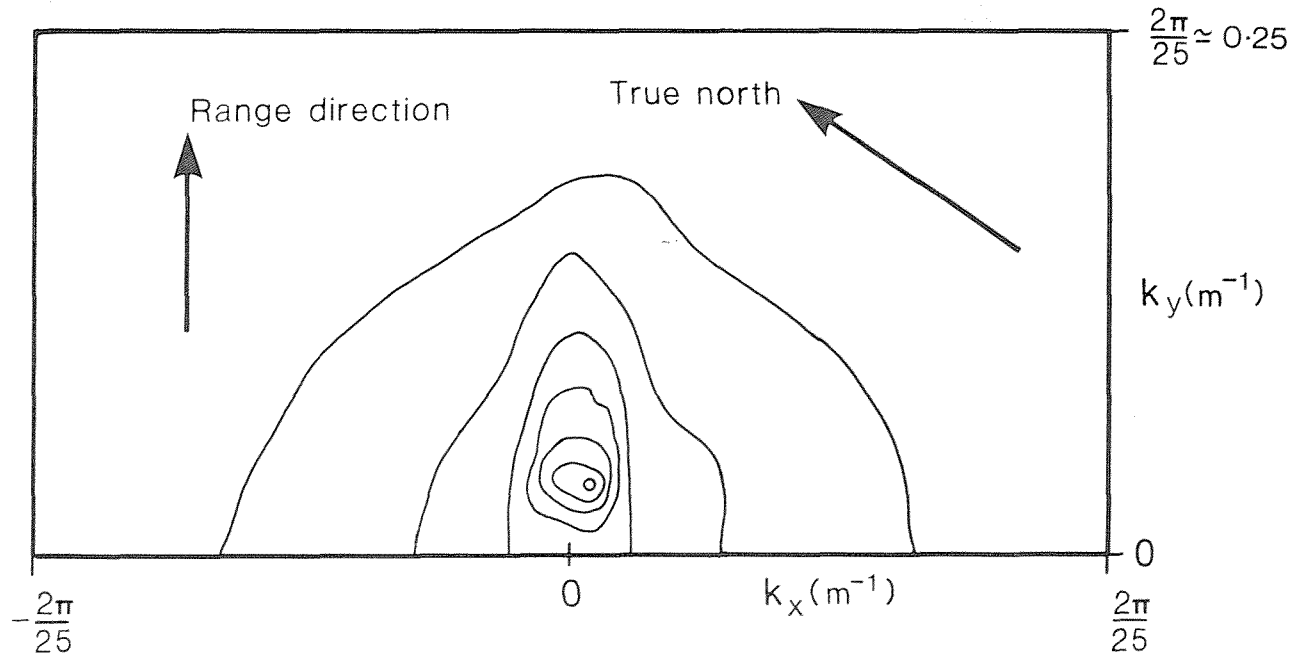

Figure 5 A Seasat SAR scene and its Fourier transform, showing the azimuthal filtering effect. The contours are at 2:1 intervals of spectral density. Details are given in the Appendix.

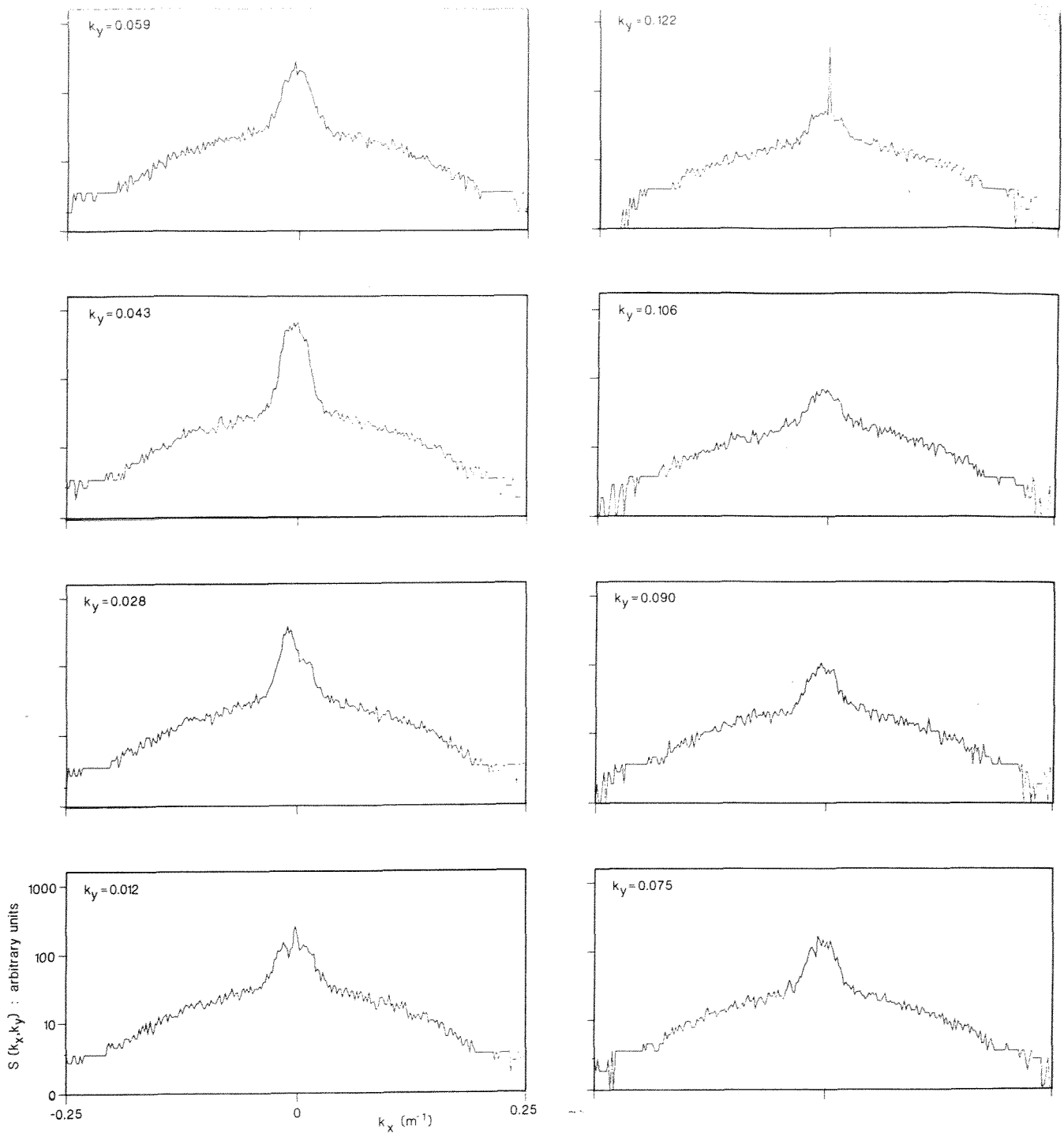

Figure 6 Eight cuts across the spectrum shown in figure 5. The plateaus visible at low spectral density correspond to the resolution intervals of the data. The spike on the spectrum for $k_y = 0.122$ is an artefact of the analyses, and has been deleted from the spectrum shown in figure 5.

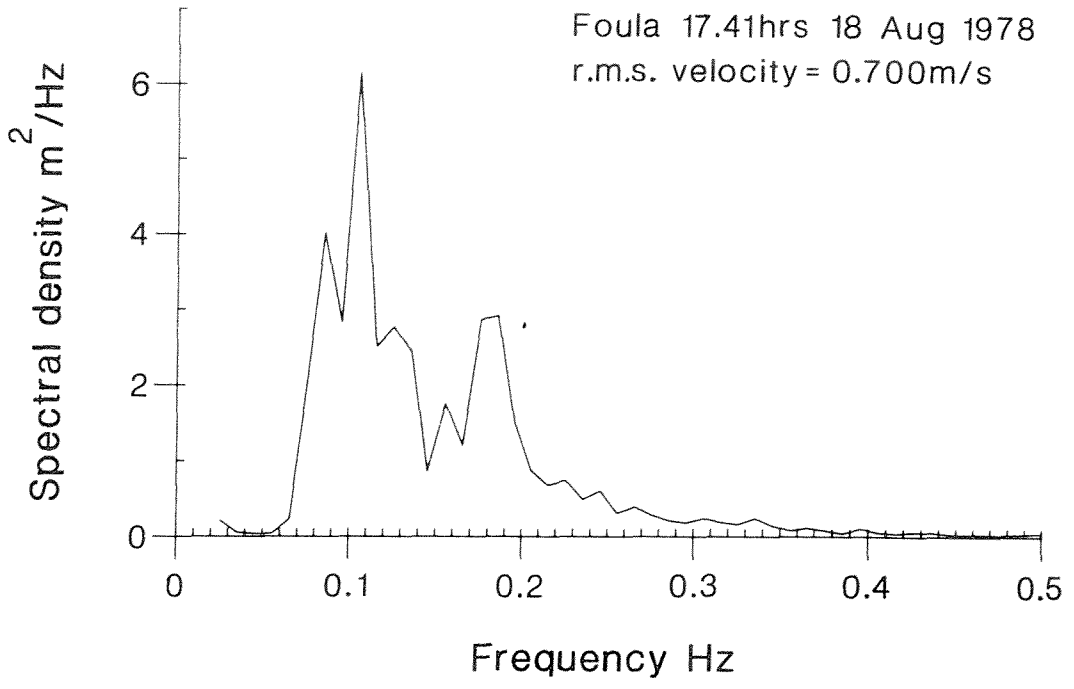

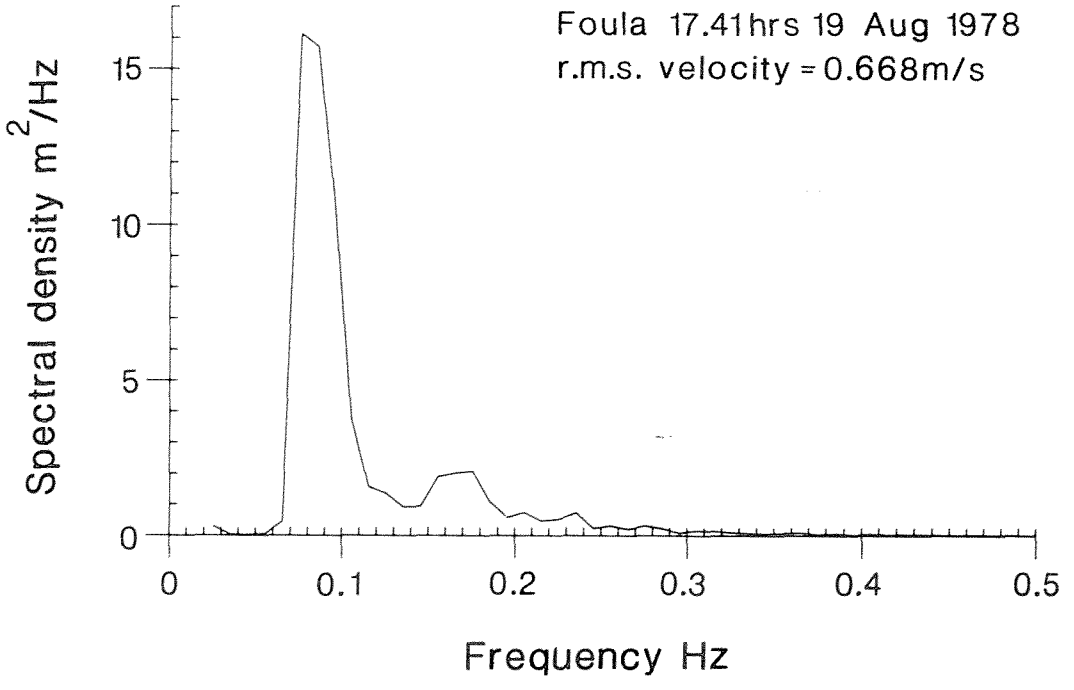

Figure 7 Wave spectra for 1741 hours 18 August and 1741 hours 19 August 1978. (Note the different ordinate scales.) The significant waveheights were 2.75 m and 3.21 m respectively.